Nanoarray-based Monolithic Adsorbers for SO₂ Removal

Junfei Weng,¹ Pu-Xian Gao^{1, *}, Zhiming Gao,² Josh Pihl,² Tim LaClair,² Mingkan Zhang,² Kyle Gluesenkamp,² and Ayyoub Momen²

Abstract

Nanoarray-based monolithic catalysts have been developed for various applications, including CO oxidation, hydrocarbon combustion, lean NO_x trapping, and low-pressure CO₂ hydrogenation. In this work, SO₂ adsorption properties have been explored and evaluated on the cordierite honeycomb monoliths grown with zinc oxide nanoarray (ZnO), zinc oxide nanoarray washcoated by BaCO₃ nanoparticles (ZnO/BaCO₃), and manganese oxide nanowire array with cryptomelane structure (MnO_x) at a temperature range from 50 °C to 425 °C. All samples showed temperaturedependent SO₂ adsorption behaviors. The adsorption results revealed the performance order: MnO_x > ZnO/BaCO₃ > ZnO, with ~90% SO₂ adsorbed in MnO_x at 425 °C. Washcoated BaCO₃ contributed to the improvement of SO₂ adsorption in ZnO nanoarray, and the best performance displayed in MnO_x may be attributed to their high specific surface area. After regeneration, nanoarrays all exhibited good thermal stability during test-regeneration cycles. No additional phase was formed in regenerated ZnO nanoarrays (ZnO-R), while BaCO₃ was converted to BaSO₄ in the regenerated ZnO/BaCO₃ nanoarrays (ZnO/BaCO₃-R), and the sulfur species (possibly MnSO₄) and Mn₂O₃ were found in regenerated MnO_x nanoarrays (MnO_x-R). It is noted that small amount of sulfur species (possibly MnSO₄) may promote the SO₂ adsorption of MnO_x-R at a lower temperature, while the formed Mn₂O₃ contributed to the deactivation of MnO_x-R.

Key words: Adsorber, SO₂ removal, Metal oxide, Nanoarray, Deactivation

1. Introduction

Sulfur dioxide (SO_2) is one of the major air pollutants resulting in the formation of acid smog and acid rain, which could significantly influence the environment and human health¹⁻³. Regulations to limit the emission of SO_2 into the atmosphere are increasingly stringent around the world. The generation of SO_2 is mainly from the burning of fossil fuels that contain sulfur, such as diesel in automobile devices and coal in the thermal power sector and steel-making industry. Because of the corrosive acidity, SO_2 is detrimental to the industrial instruments. In addition, many functional catalysts, such as three-way catalysts and NO_x trap catalysts, are sensitive to SO_2 poisoning concerning its very reactive nature⁴. It remains challenging to develop advanced catalysts with high resistance or removal capacity towards SO_2 .

¹ Nanomaterials Science Laboratory, Department of Materials Science and Engineering & Institute of Materials Science, University of Connecticut, Storrs, CT 06269-3136, USA

² Oak Ridge National Laboratory, Oak Ridge, TN 37831, USA

^{*} Corresponding author: puxian.gao@uconn.edu

Historically, employing low-cost basic oxide materials to capture SO₂ followed by the regeneration periodically at elevated temperature is one of the common strategies to remove SO₂⁵. Zinc oxide is a common sorbent for SO₂ removal in industry due to its high desulfurization stability and reaction activity⁶⁻⁸. In the past decades, substantial efforts have been invested to study the interaction of SO₂ with ZnO from both theoretical and experimental aspects. Density functional theory (DFT) calculations indicated that SO₂ poisoning could be converted on nonpolar $\{10\overline{1}0\}$ facets and the Zn-terminated (0001) polar facet was less active towards SO₂ than the O-terminated $(000\overline{1})$ polar facet⁹. Through a systematical investigation by in situ infrared and temperature programmed desorption (IR/TPD) and X-ray photoelectron spectroscopy (XPS), the SO₂ interaction with ZnO was suggested to be dependent on the acidbase property and surface structure of the polar and nonpolar facets¹⁰. On the other hand. adsorption of SO₂ on ZnO nanomaterials was also dependent on the size and shape¹¹. ZnO nanorods could adsorb 30% more than nanoparticles, as the more planar surfaces of ZnO are more favorable for the weakly adsorbed SO2, while less so for the strongly adsorbing sulfur species (sulfur, sulfide, sulfate and sulfite). Manganese oxide is another promising candidate for SO₂ removal, as it has high sulfur capture capacity and good regeneration ability¹²⁻¹³. Especially, cryptomelane (K_xMn₈O₁₆) was found to be a high-capacity sulfur oxide absorbent under oxidizing and inert conditions¹⁴⁻¹⁵. Over 250-475 °C, cryptomelane could capture up to 70 wt.% SO₂ through the oxidation of SO₂ to SO₃ by Mn⁴⁺ and Mn³⁺ followed by SO₃ reaction with Mn²⁺ to form MnSO₄. Even exposed to lean-rich cycles up to 550 °C, cryptomelane still maintained a very high SO₂ capacity.

Monolithic catalysts have been successfully implemented in many industrial applications 16 . Cordierite honeycomb is the most common monolithic substrate due to its good thermal shock resistance, mechanical durability, and low pressure drop 17 . Recently, zinc oxide nanorod 18 and manganese oxide nanowire were successfully integrated on the cordierite substrates to form nanoarray-based monolithic catalysts. These catalysts had demonstrated high material utilization efficiency, excellent thermal and mechanical stabilities. In particular, ZnO nanoarray-based catalysts showed a higher desulfurization capacity towards H_2S than ZnO powder-coated cordierite, which was attributed to the preferentially exposed ZnO nonpolar $\{10\overline{1}0\}$ facets of hexagonal wurtzite-type crystals and the strong gas-solid interactions due to the well-defined nanoarray configuration 20 .

In this paper, zinc oxide and manganese oxide nanoarray based monolithic adsorbers were synthesized and evaluated for SO_2 removal properties. Considering that the $BaCO_3$ is a common storage material used in NO_x trap catalysts, $BaCO_3$ nanoparticles were prepared by coprecipitation method and washcoated onto the ZnO nanoarray. The SO_2 adsorption behaviors of the as-prepared nanoarray based monoliths (ZnO, ZnO/BaCO₃ and MnO_x) were evaluated and re-tested after regeneration at 600 °C under N_2 atmosphere. All monoliths showed the temperature-dependent SO_2 adsorption behaviors. The SO_2 removal efficiency decreased in order: $MnO_x > ZnO/BaCO_3 > ZnO$. At 50-425 °C. MnO_x nanoarray based monoliths could adsorb up to 90% SO_2 at 425 °C during cyclic test-regeneration process, promising to be a good SO_2 removal material in the future.

2. Experimental Method

2.1. Materials

Cordierite honeycomb substrates were obtained from Corning Inc. with a cell density of 400 cpsi. Zinc acetate dihydrate $(Zn(CH_3COO)_2 \cdot 2H_2O)$, Fisher Scientific) and hexamethylenetetramine (HMT, Fisher Scientific) were used for the synthesis of zinc oxide nanoarray. Barium carbonate (BaCO₃, 99.80%, Alfa Aesar) from, sodium carbonate (Na₂CO₃, 98.8%, J. T. Baker) and ethylene glycol (Fisher Scientific) were used to prepare BaCO₃ nanoparticles. Manganese sulfate monohydrate (MnSO₄·H₂O, Sima-Aldrich), potassium chlorate (KClO₃, J. T. Baker) and sulfuric acid (H₂SO₄, 95.0-98.0%, J. T. Baker) were used for the synthesis of manganese oxide nanoarray.

2.2. Samples preparation

2.2.1. Zinc oxide nanoarray-based monoliths

Zinc oxide nanoarray were grown on the cordierite honeycomb substrate by a two-step hydrothermal synthesis method¹⁸, i.e., the deposition of ZnO seeds layer followed by hydrothermal growth of ZnO nanoarray. Typically, a pre-cleaned monolithic cordierite substrate was submerged under 20 mM zinc acetate solution in ethanol for 30 s and dried in an oven at 250 °C for 5 minutes. The seeding steps were repeated for 10 cycles, and then calcined in a furnace at 350 °C for 5 h to obtain the crystallized ZnO seeds. ZnO nanoarrays were then grown on the seeded substrate using the mixed solution of 12.5 mM zinc acetate and HMT in DI water. The synthesis was conducted at 95 °C for 2 h under strong magnetic stirring. After synthesis, ZnO nanoarrays were then dried in an oven at 90 °C overnight.

 $BaCO_3$ nanoparticles were prepared by co-precipitation method²¹. Specifically, 0.02 mol $Ba(NO_3)_2$ and 0.02 mol Na_2CO_3 were mixed in 200 mL ethylene glycol. The solution was placed in a flask at 80 °C for 1 h with strong agitation. The acquired $BaCO_3$ nanoparticles were collected and rinsed in de-ionized (DI) water, and then dried at 90 °C overnight. The obtained $BaCO_3$ nanoparticles were dispersed in dimethylformamide (DMF, Fisher Scientific) and deposited onto the ZnO nanoarray by washcoat to prepare the sample ZnO/BaCO₃. The mass loading ratio of $BaCO_3$ nanoparticles were controlled to be 10 wt.%.

2.2.2. Manganese oxide nanoarray-based monoliths

Manganese oxide nanoarray-based monoliths were prepared by a hydrothermal method ¹⁹. 90 mmol of $MnSO_4 \cdot H_2O$ and 158 mmol of $KClO_3$ were dissolved in 300 mL of DI water with 5 mL of H_2SO_4 . The mixed solution was transferred into a 400 mL capped glass bottle, and the cordierite substrate was located on the bottom. The reaction was conducted at 90 °C for 12 h to synthesize manganese oxide nanoarrays on the cordierite. After synthesis, the sample was rinsed with DI water, applied with 2 h of sonication in water, and then dried in a vacuum oven at 60 °C overnight.

2.3. Structure characterization

The X-ray diffraction (XRD) patterns were acquired using a BRUKER D2 X-ray diffractometer (Cu K α radiation, λ = 1.540598 Å) with an operating voltage of 30.0 kV, and a current of 10 mA.

The morphology and structure were characterized using a field emission scanning electron microscope (FE-SEM, FEI Teneo LoVac, 20 kV) and a high-resolution transmission electron

microscope (TEM, FEI Talos F200X S/TEM, 300 kV) attached with an energy-dispersive X-ray spectroscopy (EDS) detector for elemental mapping analysis.

The textural properties were obtained through N_2 isothermal adsorption-desorption method at 77K (ASAP 2020 volumetric adsorption analyzer, Micromeritics). Specific surface area was estimated by Brunauer-Emmett-Teller (BET) analysis, while the pore size distribution was calculated by Barrett-Joyner-Halenda (BJH) model.

2.4. SO₂ adsorption performance test

The SO_2 adsorption properties were evaluated in a horizontal quartz tube reactor. Each sample with a volume of $0.8~cm \times 0.8~cm \times 1~cm$ was used. The feed gas was composed of SO_2 (20 ppm), NO (40 ppm), O_2 (2%), CO_2 (8%) and N_2 balanced. The space velocity was maintained at ~15,000 h⁻¹. Fourier Transform infrared spectrometer (FTIR, Thermo-fisher Nicolet 6700), calibrated for SO_2 , was used for on-line gas analysis. At the beginning of the experiment, the furnace was maintained at 50 °C. The inlet reactant gases were bypassing the reactor firstly, and switched back to the reactor line until the gas component was stable. After switch, the reactor was initially kept at 50 °C for 20 min, then heated to 425 °C with a ramping rate of 10 °C/min. Each sample was maintained at 225 °C, 275 °C, 325 °C, 375 °C, and 425 °C for 20 min. After the first-run evaluation, samples were regenerated under N_2 atmosphere with a flow rate of 200 sccm at 600 °C for 2 h, and then cooled down to 50 °C. Second SO_2 -removal test was run again followed by another regeneration process. After two test-regeneration cycles, the regenerated samples and fresh samples were characterized.

The SO₂ adsorption ratio at certain temperature was defined as:

$$X_{SO_2} = \frac{C_0 - C_T}{C_0} \times 100\%$$
,

where C_0 is the initial SO₂ concentration and C_i is the SO₂ concentration at the temperature T.

As stated at the beginning, for terminology convenience, the fresh nanoarray-based monolithic adsorbers were marked as ZnO, ZnO/BaCO $_3$ and MnO $_x$, while the adsorbers after regeneration were marked as ZnO-R, ZnO/BaCO $_3$ -R and MnO $_x$ -R.

3. Results

3.1. Physical Characteristics

3.1.1. SEM imaging

The morphologies of fresh samples were investigated by SEM imaging. Figure 1a-b revealed the successful integration of ZnO nanoarray onto the channel wall surfaces of cordierite honeycomb substrate. Oriented ZnO nanorods align vertically and distribute uniformly on the cordierite surface. The diameter and thickness of ZnO nanorod array are around 140 nm and 4 μ m, respectively. The interspaces among ZnO nanorods enable the ZnO nanoarray a promising candidate for loading metal oxide.

The prepared BaCO₃ nanoparticles are deposited onto the ZnO nanoarrays with a loading amount of 10 wt.%. The BaCO₃ nanoparticles of a size of around 120 nm were confirmed by TEM

imaging with selective area diffraction analysis (not shown here). As shown in Figure 1c-d, BaCO $_3$ nanoparticles are initially distributed within the layer of ZnO nanoarray due to its nano-scale particle size, and then accumulate to form interconnected larger particles (< 1 μ m) on the surface of ZnO nanoarrays once the interspaces of ZnO nanoarray are filled up.

Manganese oxide nanoarrays are also grown vertically on the cordierite surface with nanowire morphology, as presented in Figure 1e-f. The as-grown MnO_x nanowires exhibit a diameter of around 50 nm and a length of around 5 μ m.

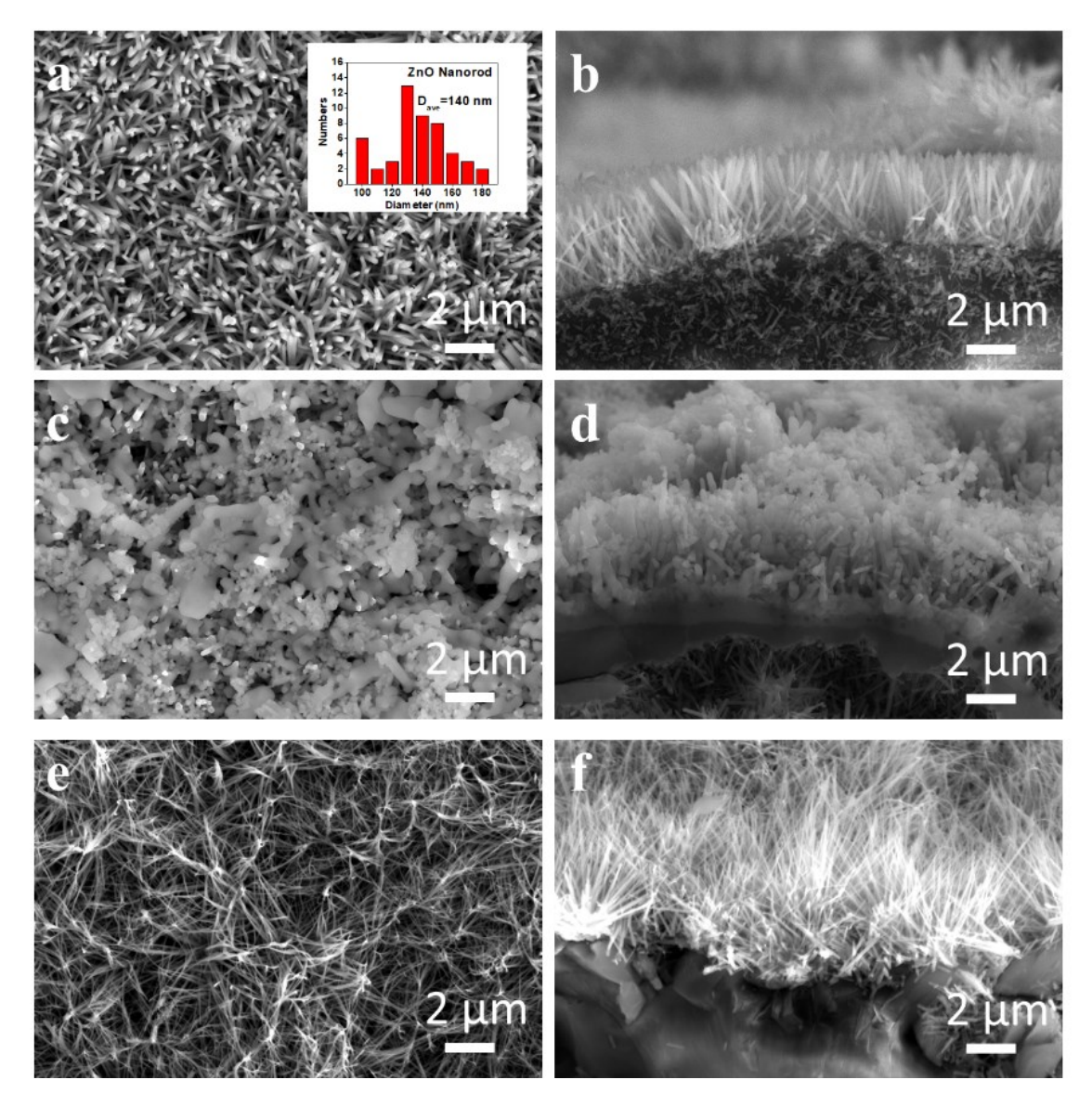


Figure 1. SEM images of fresh nanoarray monolith samples. (a, b) ZnO nanoarray (Inset: Diameter distribution of ZnO nanorods); (c, d) ZnO nanoarray washcoated by $BaCO_3$ nanoparticles (ZnO/BaCO₃); (e, f) Manganese oxide nanoarray (MnO_x). (a, c, e) Top view; (b, d, f) Cross-sectional view.

After SO₂ removal test and regeneration process, the morphologies of regenerated samples are shown in Figure 2. The morphology of ZnO nanorod maintains and the size of ZnO nanorod does not change in ZnO-R, indicating a good thermal stability of ZnO nanoarray structure. For

 $ZnO/BaCO_3$, the accumulated $BaCO_3$ particles on the surface of ZnO nanoarray in $ZnO/BaCO_3$ -R show smaller size but uniform size distribution, while cracks occur through the deposition layer. In terms of MnO_x nanoarray, in addition to the remained nanowire morphologies, new particles of around 0.27 μ m in diameter are distributed at the tips of the nanowire. EDS confirms the existence of sulfur element (2.2 at.%) in these particles, indicating that these S-containing particles are formed during the SO_2 removal test and did not decompose by the regeneration.

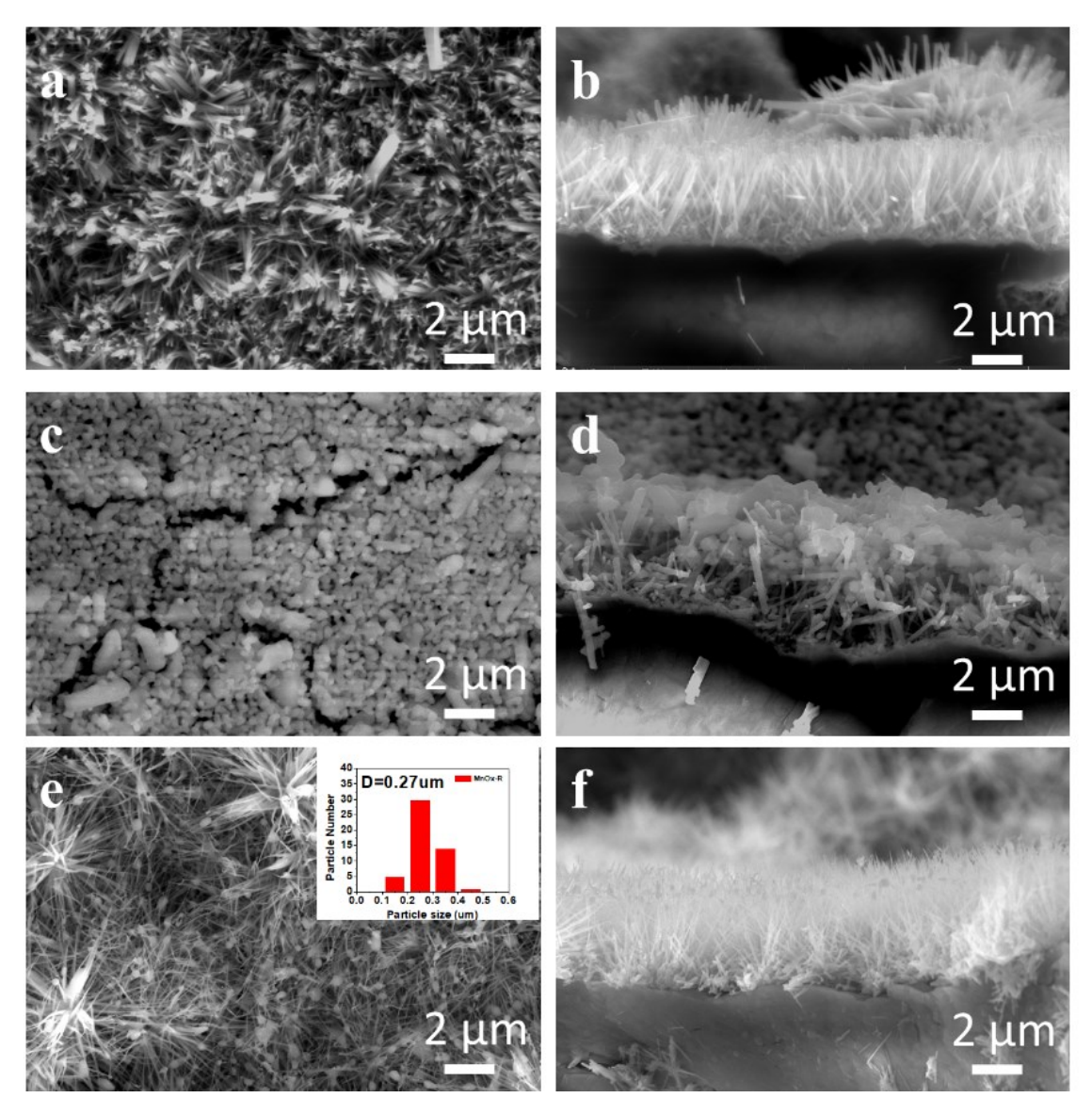


Figure 2. SEM images of regenerated samples. (a, b) ZnO nanoarray (ZnO-R); (c,d) ZnO nanoarray washcoated by $BaCO_3$ nanoparticles (ZnO/BaCO₃-R); (e, f) Manganese oxide nanoarray (MnO_x-R). (a, c, e) Top view; (b, d, f) Cross-section view.

3.1.2. X-ray diffraction analysis (XRD)

The crystal structure of fresh and regenerated samples are identified by XRD, as shown in Figure 3. As substrate is involved during the XRD test, part of XRD pattern for as-prepared adsorbers may be overlapped with the signals from cordierite substrate. ZnO (JCPDS 89-0510) is indexed in

ZnO nanoarray based samples. After regeneration, there is no additional phase identified. In ZnO/BaCO₃, both ZnO and BaCO₃ (JCPDS 05-0378) are indexed. BaSO₄ (JCPDS 26-0191) is found in ZnO/BaCO₃-R, indicating the formation of BaSO₄ during SO₂ removal. In addition, MnO_x nanoarrays are composed of cryptomelane structure (KMn₈O₁₆, JCPDS 29-1020) with an estimated crystallite size of 53.5nm calculated by Scherrer equation. In MnO_x-R, besides cryptomelane structure, another new phase of Mn₂O₃ (JCPDS 73-1826) is identified. The estimated crystallite size of cryptomelane structure is around 27.8 nm.

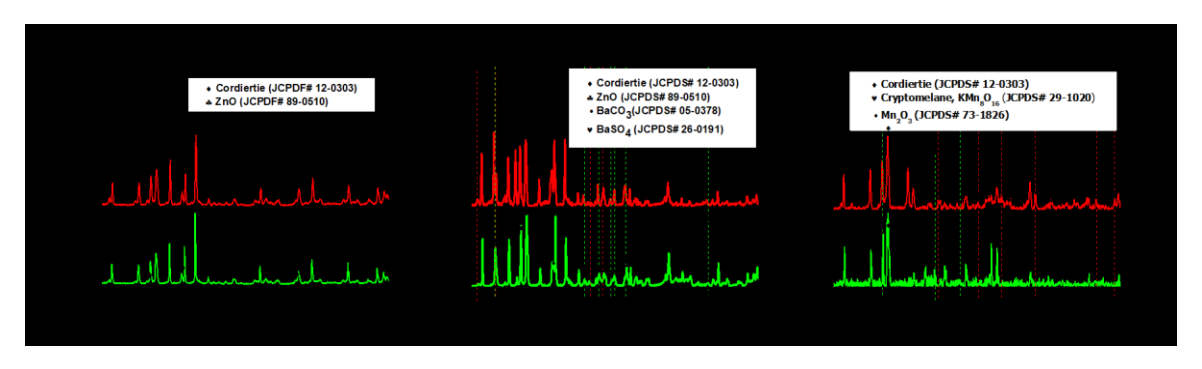


Figure 3. X-ray diffraction patterns of fresh and regenerated nanoarray monolith samples. (a) ZnO and ZnO-R; (b) $ZnO/BaCO_3$ and $ZnO/BaCO_3$ -R; (c) $ZnO/BaCO_3$ and $ZnO/BaCO_3$ -R; (c) $ZnO/BaCO_3$ -R; (d) $ZnO/BaCO_3$ -R; (e) $ZnO/BaCO_3$ -R; (e) $ZnO/BaCO_3$ -R; (f) $ZnO/BaCO_3$ -R; (e) $ZnO/BaCO_3$ -R; (f) $ZnO/BaCO_3$ -R;

3.1.3. Texture properties

Figure 4 displays the N_2 adsorption-desorption isotherms and the related BJH pore size distribution of fresh and regenerated nanoarray samples. The cordierite substrate was included during the test, while itself has a minimum specific surface area. As listed in **Table 1**, the specific surface area of ZnO, ZnO/BaCO₃ and MnO_x were 2, 2 and 30, respectively. After two test-regeneration cycles, the specific surface area of ZnO-R and ZnO/BaCO₃-R remain similar with fresh samples, but the specific surface area of MnO_x-R decreased from 30 m²/g to 2 m²/g. In addition, the micropores volume in MnO_x decreases dramatically considering the collapse of micropores during regeneration.

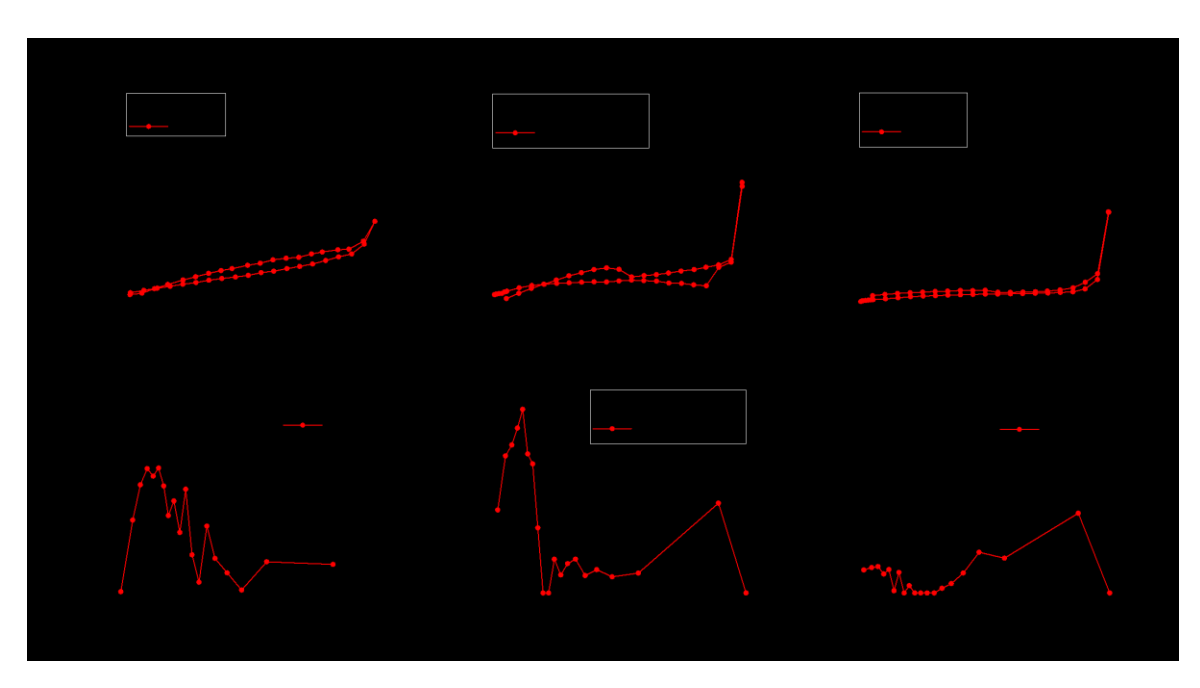


Figure 4. (a-c) N_2 adsorption-desorption isotherms and (d-f) BJH pore size distribution of fresh and regenerated nanoarray monolith samples. (a, d) ZnO and ZnO-R; (b, e) ZnO/BaCO₃ and ZnO/BaCO₃ -R; (c, f) MnO_x and MnO_x-R.

Table 1. Texture properties of fresh and regenerated nanoarray monolith samples (*cordierite substrate included)

Sample	Condition	Crystal Structure	Specific Surface Area (m²/g)*
ZnO	Fresh	ZnO	2
ZnO-R	Regenerated	ZnO	2
ZnO/BaCO ₃	Fresh	ZnO/BaCO ₃	2
ZnO/BaCO ₃ -R	Regenerated	ZnO/BaCO ₃ /BaSO ₄	2
MnO_{x}	Fresh	KMn ₈ O ₁₆	30
MnO _x -R	Regenerated	KMn_8O_{16}/Mn_2O_3	2

3.2. SO₂ adsorption performance

Figure 5 displays the SO_2 adsorption performance of as-prepared adsorbers over the temperature from 50 °C to 425 °C. After the feed gas was introduced, all samples adsorb SO_2 at 50 °C, and their SO_2 adsorption behaviors are influenced by the temperature. After dwelling at the temperature of 225 °C, 275 °C, 325 °C, 375 °C and 425 °C for 20min, the SO_2 adsorption ratio is calculated for the performance comparison between different samples.

As shown in Figure 5d-f, the SO_2 adsorption of fresh ZnO nanoarray maintains similar (7%) from 225 °C to 425 °C. After first test-regeneration cycle, the SO_2 adsorption performance in regenerated ZnO-R improves. ZnO-R adsorbs 10% SO_2 at 225 °C and then increases to 20% at 425 °C. When $BaCO_3$ nanoparticles are washcoated onto the ZnO nanoarray, SO_2 adsorption in $ZnO/BaCO_3$ shows temperature-dependence. Initially, only 5% SO_2 is adsorbed at 225 °C. As the

temperature increases, the adsorbed SO_2 increases gradually to 15% at 375 °C, and then dramatically jumps to 40% at 425 °C. The regenerated $ZnO/BaCO_3$ -R shows improved SO_2 adsorption when the temperature is lower than 375 °C, but the maximum SO_2 adsorption at 425 °C is slightly smaller than that of $ZnO/BaCO_3$. The SO_2 adsorption in MnO_x also shows positively dependence on the temperature. As temperature increases, adsorbed SO_2 increases from 7% at 225 °C to 90% at 425 °C. Regenerated MnO_x -R shows improved SO_2 adsorption at the temperature lower than 325 °C, and then remains similar performance at 325-425 °C.

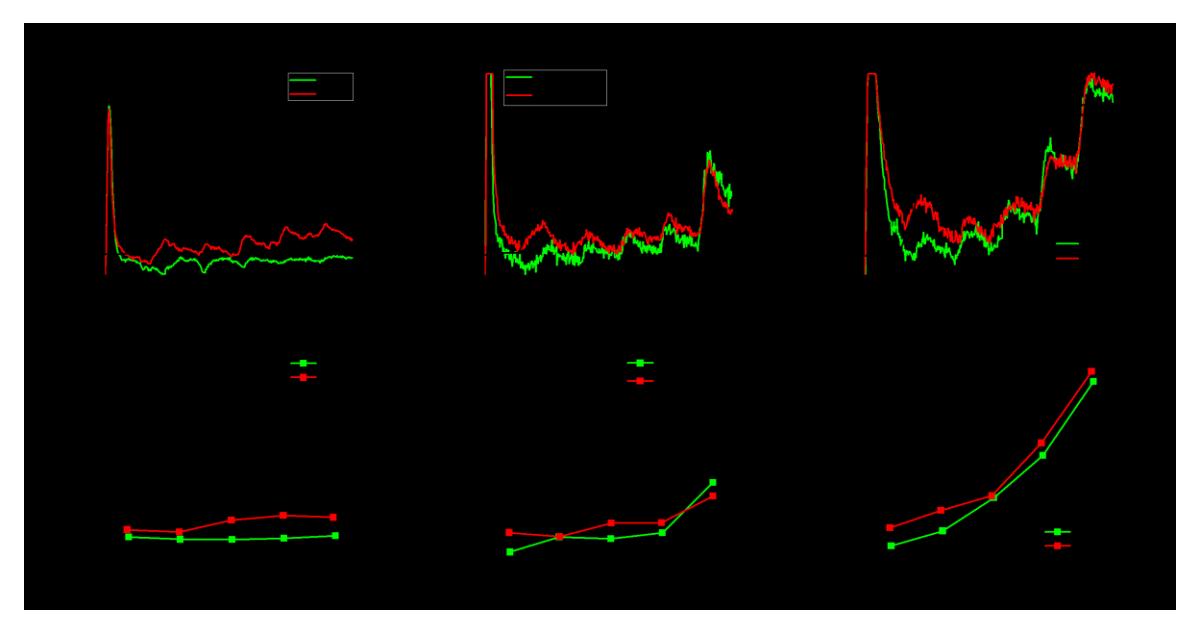


Figure 5. SO_2 removal performance of fresh and regenerated nanoarray monolith samples: (a-c) SO_2 adsorption ratio (%) vs. Time (min); (d-f) SO_2 adsorption ratio (%) vs. Temperature (°C). (a, d) ZnO and ZnO-R; (b, e) ZnO/BaCO₃ and ZnO/BaCO₃-R; (c, f) MnO_x and MnO_x-R.

Based on the above results, MnO_x shows the best SO_2 adsorption among three samples, and achieved highest adsorption at 425 °C (~90%). Therefore, the breakthrough tests of SO_2 adsorption are further conducted on MnO_x and MnO_x -R at 425 °C. As shown in Figure 6, both MnO_x and MnO_x -R could adsorb 100% SO_2 at the first 10 min after the feed gas is switched to the samples. After that, the amount of adsorbed SO_2 in MnO_x gradually decreases to 80% after 5 h, while the adsorption in MnO_x -R quickly dropped to 50% after being exposed in the reactant gas for 2.5 h.

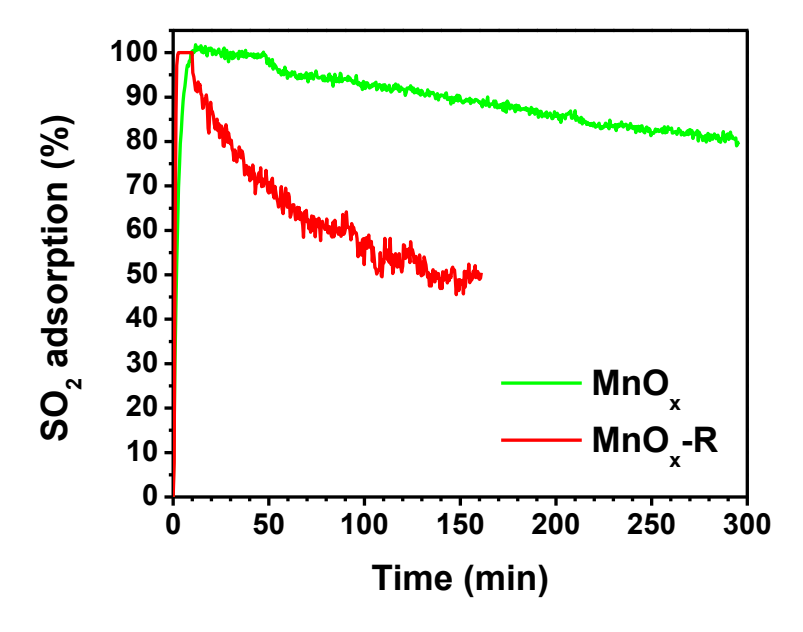


Figure 6. Breakthrough curve for SO₂ removal test on MnO_x and MnO_x-R nanoarray monolith samples at 425 °C.

4. Discussion

The mechanisms for SO_2 adsorption on metal oxides usually consist of the following three steps²²: (i) SO_2 molecules are chemisorbed on the active sites of the metal oxide to form an unstable sulfite ion; (ii) these sulfite ions further stabilize itself into a sulfite or oxidized with adsorbed oxygen or gas-phase oxygen to a sulfate form; (iii) sulfate or sulfite are decomposed with evolution of SO_3 , which could be represented by the following equations:

$$MeO(s) + SO_2(g) \leftrightarrow MeSO_3^*(ads)$$
 (i-1)

$$O_2(g) \stackrel{MeO}{\longleftrightarrow} 2O^*(ads)$$
 (ii-1)

$$MeSO_3^*(ads) + O^*(ads) \rightarrow MeSO_4(s)$$
 (ii-2)

$$MeSO_3^*(ads) \leftrightarrow MeSO_3(s)$$
 (ii-3)

$$MeSO_3^*(ads) \to Me^*(s) + SO_3(g)$$
 (iii-1)

$$MeSO_4(s) \rightarrow MeO(s) + SO_3(g)$$
 (iii-2)

$$2 Me^*(s) + O_2(g) \rightarrow 2 MeO(s)$$
 (iii-3)

It is noted that when the temperature is above the sulfate decomposition temperature, metal oxides could also behave as catalysts as all three steps (i, ii, and iii) could occur in sequence. However, little or no catalytic activity can be detected for metal oxides below the sulfate decomposition temperature. In addition, the adsorption kinetics of SO₂ on metal oxides are influenced by the external and internal mass transfers, including the pore diffusion and solid-

phase diffusion. Meanwhile, above the sulfate decomposition temperature, metal oxide could encounter more severe sintering effect, thus influencing the cyclic SO₂ adsorption performance⁵. On the other hand, through impurity doping in metal oxides could help decrease the sulfate decomposition temperature, thus decrease the catalytic temperature window and favor for low temperature adsorption. Therefore, the performance of SO₂ adsorption on the metal oxides could be influenced by the temperature, specific surface area, and intrinsic activity nature.

In this work, all samples exhibit positive temperature-dependent SO_2 adsorption, especially MnO_x and MnO_x -R. During the adsorption, the specific surface area and pore size should also be considered, affecting the gas diffusion and accessibility during reaction. MnO_x exhibits higher SO_2 adsorption due to their higher specific surface area and more micropores than ZnO and $ZnO/BaCO_3$. When the temperature increases, the activity nature of different metal oxides is more important. At 425 °C, SO_2 adsorption efficiencies of ZnO, $ZnO/BaCO_3$ and MnO_x are 7%, 40% and 90%, respectively. In addition to SO_2 adsorbed by ZnO, the washcoated $BaCO_3$ could interact with SO_2 to form $BaSO_4$. The cryptomelane nanowire is reported to exhibit abundant surface-adsorbed oxygen and lattice oxygen¹⁹, which could promote the oxidation of SO_2 to SO_3 and improve the SO_2 adsorption.

Various sulfur species could be formed when the metal oxides are exposed to SO2, which requires a following high-temperature regeneration to decompose those formed species. In this work, no additional phase except ZnO is detected on ZnO nanoarray after regeneration and the adsorption performance is recovered. There may be two possible reasons. Firstly, a phase diagram indicated that the reaction between ZnO and SO₂ will only occur under high oxygen and SO_2 partial pressures at a specific temperature²³. The low level of SO_2 concentration in the current work could not trigger the reaction. Secondly, ZnO tends to form sulfate when preferentially exposed ($10\overline{1}0$) facets in ZnO nanoarray interact with SO₂, but the formed sulfate would be decomposed at 600 °C during regeneration²⁴. For ZnO/BaCO₃-R, additional phase of BaSO₄ is identified as BaSO₄ is thermodynamically stable over 800 °C²⁵. The as-formed BaSO₄ could not be able to convert back to BaCO₃ at the current regeneration temperature. In terms of MnO_x-R , S-containing species (S in 2.2 at.%) is found by SEM/EDX and Mn_2O_3 is identified by XRD. Sulfur-containing species, possibly MnSO₄, form during SO₂ adsorption test and could not be completely decomposed during regeneration process. It is reported that the removal of SO₂ by MnO₂-modified activated coke could be improved with an appropriate amount of MnSO₄, as Mn²⁺ in the produced MnSO₄ could form new liquid-phase in the presence of water to simultaneously promote SO₂ removal with the solid-phase catalyst (activated coke), but an excessive amount of MnSO₄ could block the access of SO₂ to the pore network of solid-phase catalysis, hampered the adsorption activity²⁶. This may be the reason why the SO₂ adsorption in MnO_x-R is improved at temperatures lower than 325 °C, but the SO₂ adsorption performance in MnO_v decreases gradually in the long-term breakthrough test. In addition, Mn₂O₃ that may be from the partial decomposition of MnSO₄, showing the poorest SO₂ removal ability²⁷. This could explain why the MnO_x-R quickly dropped to 50% SO₂ adsorption within 2.5 h.

5. Conclusion

In this work, zinc oxide nanorod (ZnO), zinc oxide nanorod washcoated by BaCO $_3$ nanoparticles (ZnO/BaCO $_3$), and manganese oxide nanowire (MnO $_x$) with cryptomelane structure were prepared and evaluated for SO $_2$ adsorption behaviors at 50-425 °C. The adsorption performances of the tested samples decrease in order: MnO $_x$ > ZnO/BaCO $_3$ > ZnO, and are positively dependent on test temperature. MnO $_x$ nanoarrays show the highest SO $_2$ adsorption efficiency of 90% at 425 °C. After two test-regeneration cycles, nanoarray structure showed good thermal stability. The formation of Mn $_2$ O $_3$ during the test-regeneration cycles leads to the fast deactivation of MnO $_x$ -R towards SO $_2$ adsorption in the breakthrough test. Our investigation provides another promising candidate of MnO $_x$ nanoarray based monoliths towards SO $_2$ removal, and the interaction between SO $_2$ and MnO $_x$ nanowires with cryptomelane structure during test-regeneration process will be further explored.

Acknowledgement

This work was sponsored by the U.S. DOE Building Technologies Office, with Antonio Bouza as a program manager, and the U.S. National Science Foundation. J. Weng was partially supported by the Thermo Fisher Scientific Graduate Fellowship. The microscopy studies were performed using the facilities in the UConn/Thermo Fisher Scientific Center for Advanced Microscopy and Materials Analysis (CAMMA).

References

- 1. Greenberg, N.; Carel, R. S.; Derazne, E.; Bibi, H.; Shpriz, M.; Tzur, D.; Portnov, B. A., Different effects of long-term exposures to SO2 and NO2 air pollutants on asthma severity in young adults. *Journal of Toxicology and Environmental Health, Part A* **2016**, *79* (8), 342-351.
- 2. Kan, H.; Wong, C.-M.; Vichit-Vadakan, N.; Qian, Z., Short-term association between sulfur dioxide and daily mortality: The Public Health and Air Pollution in Asia (PAPA) study. *Environmental Research* **2010**, *110* (3), 258-264.
- 3. Weerasinghe, S., A missing values imputation method for time series data: an efficient method to investigate the health effects of sulphur dioxide levels. *Environmetrics: The official journal of the International Environmetrics Society* **2010**, *21* (2), 162-172.
- 4. Choi, J.-S.; Partridge, W. P.; Pihl, J. A.; Daw, C. S., Sulfur and temperature effects on the spatial distribution of reactions inside a lean NOx trap and resulting changes in global performance. *Catalysis Today* **2008**, *136* (1), 173-182.
- 5. Mathieu, Y.; Tzanis, L.; Soulard, M.; Patarin, J.; Vierling, M.; Molière, M., Adsorption of SOx by oxide materials: A review. *Fuel Processing Technology* **2013**, *114*, 81-100.
- 6. Pineda, M.; Palacios, J.; Alonso, L.; Garcia, E.; Moliner, R., Performance of zinc oxide based sorbents for hot coal gas desulfurization in multicycle tests in a fixed-bed reactor. *Fuel* **2000**, *79* (8), 885-895.
- 7. Sasaoka, E.; Hirano, S.; Kasaoka, S.; Sakata, Y., Stability of zinc oxide high-temperature desulfurization sorbents for reduction. *Energy & Fuels* **1994**, *8* (3), 763-769.
- 8. Siriwardane, R. V.; Cicero, D. C.; Jain, S.; Gupta, R. P.; Turk, B. S. *Durable zinc oxide-based regenerable sorbents for desulfurization of syngas in a fixed-bed reactor*; National Energy Technology Laboratory, Morgantown, WV; Research Triangle ...: 2002.
- 9. Prades, J.; Cirera, A.; Morante, J., Ab initio calculations of NO2 and SO2 chemisorption onto non-polar ZnO surfaces. *Sensors and Actuators B: Chemical* **2009**, *142* (1), 179-184.
- 10. Luo, S.; Liu, J.; Wu, Z., Interaction of SO2 with ZnO Nanoshapes: Impact of Surface Polarity. *The Journal of Physical Chemistry C* **2019**.
- 11. Wu, C.-M.; Baltrusaitis, J.; Gillan, E. G.; Grassian, V. H., Sulfur Dioxide Adsorption on ZnO Nanoparticles and Nanorods. *The Journal of Physical Chemistry C* **2011**, *115* (20), 10164-10172.
- 12. Wang, J.; Liang, B.; Parnas, R., Manganese-based regenerable sorbents for high temperature H2S removal. *Fuel* **2013**, *107*, 539-546.
- 13. Wang, H. Q.; Ju, S. G.; Liu, L. P.; Zhao, X. W.; Mi, J. In *The Regeneration properties of Manganese Oxide Sorbent under SO2 Atmosphere*, Materials Science Forum, Trans Tech Publ: 2016; pp 140-145.
- 14. Li, L.; King, D. L., High-Capacity Sulfur Dioxide Absorbents for Diesel Emissions Control. *Industrial & Engineering Chemistry Research* **2005**, *44* (1), 168-177.
- 15. Li, L.; King, D. L., Cryptomelane as high-capacity sulfur dioxide absorbent for diesel emission control: A stability study. *Industrial & engineering chemistry research* **2005**, *44* (19), 7388-7397.
- 16. Weng, J.; Lu, X.; Gao, P. X., Nano-array integrated structured catalysts: A new paradigm upon conventional wash-coated monolithic catalysts? *Catalysts* **2017**, *7* (9).
- 17. Elmer, T. H., Ultra-low expansion ceramic articles. Google Patents: 1976.
- 18. Xiao, W.; Guo, Y.; Ren, Z.; Wrobel, G.; Ren, Z.; Lu, T.; Gao, P.-X., Mechanical-agitation-assisted growth of large-scale and uniform ZnO nanorod arrays within 3D multichannel monolithic substrates. *Crystal Growth & Design* **2013**, *13* (8), 3657-3664.

- 19. Liu, Z.; Wu, D.; Ren, S.; Chen, X.; Qiu, M.; Wu, X.; Yang, C.; Zeng, G.; Sun, Y., Solvent-Free Synthesis of c-Axis Oriented ZSM-5 Crystals with Enhanced Methanol to Gasoline Catalytic Activity. *ChemCatChem* **2016**, *8* (21), 3317-3322.
- 20. Wang, S.; Wu, Y.; Miao, R.; Zhang, M.; Lu, X.; Zhang, B.; Kinstler, A.; Ren, Z.; Guo, Y.; Lu, T.; Suib, S. L.; Gao, P. X., Scalable continuous flow synthesis of ZnO nanorod arrays in 3-D ceramic honeycomb substrates for lowerature desulfurization. *CrystEngComm* **2017**, *19* (34), 5128-5136.
- 21. Thongtem, T.; Tipcompor, N.; Phuruangrat, A.; Thongtem, S., Characterization of SrCO3 and BaCO3 nanoparticles synthesized by sonochemical method. *Materials Letters* **2010**, *64* (4), 510-512.
- 22. Koballa, T. E.; Dudukovic, M. In *Sulfur dioxide adsorption on metal oxides supported on alumina*, AIChE Symposium Series, 1977; pp 199-228.
- 23. Cheng, S.; Søgaard, M.; Han, L.; Zhang, W.; Chen, M.; Kaiser, A.; Hendriksen, P. V., A novel CO2- and SO2-tolerant dual phase composite membrane for oxygen separation. *Chemical Communications* **2015**, *51* (33), 7140-7143.
- 24. Ostroff, A. G.; Sanderson, R. T., Thermal stability of some metal sulphates. *Journal of Inorganic and Nuclear Chemistry* **1959**, *9* (1), 45-50.
- 25. Lietti, L.; Forzatti, P.; Nova, I.; Tronconi, E., NOx Storage Reduction over Pt-Ba/γ-Al2O3 Catalyst. *Journal of catalysis* **2001**, *204* (1), 175-191.
- 26. Yang, L.; Jiang, X.; Yang, Z.-S.; Jiang, W.-J., Effect of MnSO4 on the Removal of SO2 by Manganese-Modified Activated Coke. *Industrial & Engineering Chemistry Research* **2015**, *54* (5), 1689-1696.
- 27. Qu, Y.-F.; Guo, J.-X.; Chu, Y.-H.; Sun, M.-C.; Yin, H.-Q., The influence of Mn species on the SO2 removal of Mn-based activated carbon catalysts. *Applied Surface Science* **2013**, *282*, 425-431.